Current Optics and Photonics
Vol. 4, No. 5, October 2020, pp. 421-427

ISSN: 2508-7266(Print) / ISSN: 2508-7274(Online)
DOI: https://doi.org/10.3807/COPP.2020.4.5.421

A Privacy-protection Device Using a Directional Backlight and Facial Recognition

Hyeontaek Lee, Hyunsoo Kim, and Hee-Jin Choi*

Department of Physics and Astronomy, Sejong University, Seoul 05006, Korea

(Received September 2, 2020 : revised September 14, 2020 : accepted September 14, 2020)

A novel privacy-protection device to prevent visual hacking is realized by using a directional backlight and facial recognition. The proposed method is able to overcome the limitations of previous privacy-protection methods that simply restrict the viewing angle to a narrow range. The accuracy of user tracking is accomplished by the combination of a time-of-flight sensor and facial recognition with no restriction of detection range. In addition, an experimental demonstration is provided to verify the proposed scheme.

Keywords : Privacy protection, Directional backlight, Face detection range
OCIS codes : (110.2990) Image formation theory; (110.1085) Adaptive imaging

I. INTRODUCTION

With rapid progress in display technologies to provide wider viewing angle and higher contrast, the information displayed on a device's screen can be seen from anywhere by anybody more easily. Therefore, *visual hacking* to steal essential information on a screen, by peeping on it or capturing it using a telephoto lens, has become much easier and more common [1]. To prevent the visual hacking described above, there have been some methods to restrict the viewing angle within a narrow range [2-4]. However, those kinds of methods are still vulnerable to visual hacking, since they cannot distinguish the original user from the visual hacker. Moreover, since those conventional protections are not switchable, the user can feel uncomfortable due to the narrower viewing angle, even with a situation that no protection is required. In this paper, we propose a novel privacy-protection technique to adopt a directional backlight and facial-recognition system with higher accuracy and extended detection range, by combining a time-of-flight (TOF) sensor with facial recognition. An experimental demonstration is also provided to verify the proposed scheme.

II. PRINCIPLE

2.1. Facial Recognition Closer than the Minimum Detection Range of the TOF Sensor

To converge the light rays from the display device to the position of the face of the user, it is necessary to acquire the coordinates of that face. For that purpose, a TOF sensor such as the Kinect V2 is commonly used to measure the depth map. However, the TOF sensor has the limitation of a minimum detection range, which means that it cannot detect an object closer than that range. Since that range is about 0.7 m in the case of the Kinect V2 [5], we propose a novel method to extend the range of depth detection by combining a color image and a depth map.

At first, the facial recognition requires a color image of the face, which is provided by a color-image sensor besides the TOF sensor. Thus a calibration between the color image and depth map is necessary. Though a method using a checkerboard is commonly used [6], we used Kinect for Windows SDK 2.0 functions for this study, since we think that it is not practical for the user to always carry a checkerboard for calibration. Nevertheless, any kind of calibration method can be used if the output is accurate.

After the calibration is finished, in order to calculate the real coordinates (x, y) of the face's center, we must determine a single pixel located at a particular depth z

*Corresponding author: hjchoi@sejong.ac.kr, ORCID 0000-0002-6482-9358
Color versions of one or more of the figures in this paper are available online.

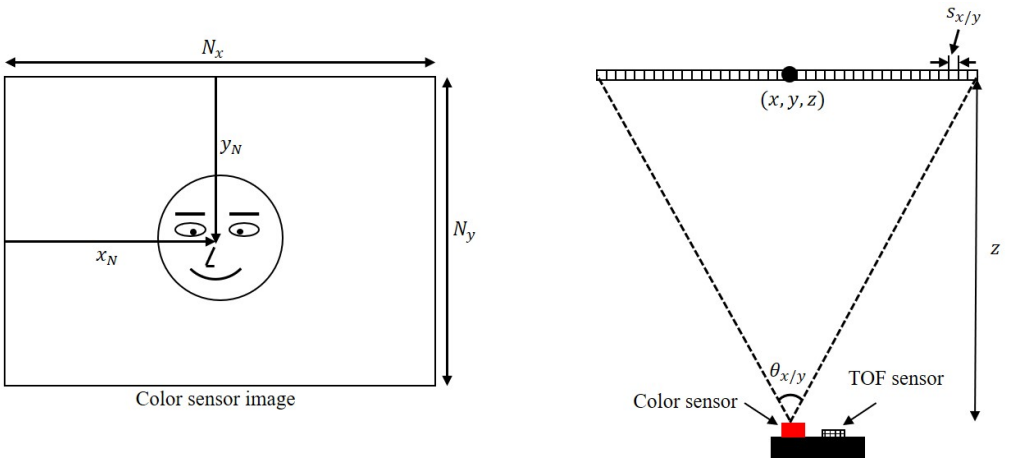

FIG. 1. Calculation of the true position of the face's center.

with horizontal/vertical sizes of $s_{x/y}$ as follows, with horizontal/vertical field of view $\theta_{x/y}$ and resolution $N_{x/y}$ of the color sensor, and depth z measured by the TOF sensor as shown in Fig. 1.

$$s_{x/y} = \frac{2z\tan\left(\frac{\theta_{x/y}}{2}\right)}{N_{x/y}}. \tag{1}$$

Using the above equation and the calibrated pixel coordinates of the face's center (x_N, y_N), we can acquire the three-dimensional coordinates of the face's center (x, y, z) as follows:

$$(x, y, z) = \left(\left(x_N - \frac{N_x}{2}\right)\frac{2z\tan\left(\frac{\theta_x}{2}\right)}{N_x}, \left(y_N - \frac{N_y}{2}\right)\frac{2z\tan\left(\frac{\theta_y}{2}\right)}{N_y}, z\right). \tag{2}$$

However, as described above, this technique can be used only when the face's center is beyond the minimum detection range of the TOF sensor. Thus we propose a novel method to retrieve the depth from the distance between the eyes of the observer after an initial recognition of the face's position.

When the initial recognition of the face's position is finished, the number of pixels N_{eye_i} between the eyes of the observer is saved with the initial depth z_i as shown Fig. 2. Then we can derive the equation below from Fig. 2, because the distance between the eyes is fixed.

$$s_{x_i} N_{eye_i} = s_x N_{eye}. \tag{3}$$

Since the horizontal size of a single pixel is proportional to the depth of the face's center, as described in Eq. (1), we can replace s_{x_i} and s_x in Eq. (3) with z_i and z as below, respectively.

$$z = \frac{N_{eye_i}}{N_{eye}} z_i. \tag{4}$$

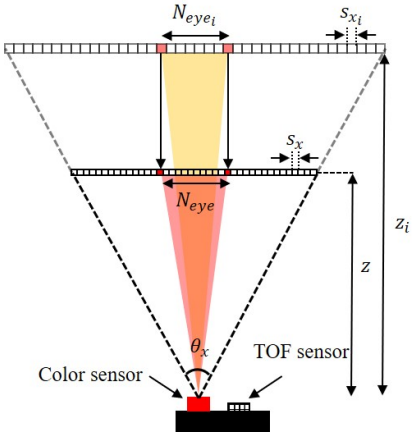

FIG. 2. Retrieving the depth z of the face's center without the output from the TOF sensor.

Thus, without the output from the TOF sensor, the depth z of the face position can be retrieved by only obtaining the number of pixels N_{eye} between the eyes from the color image sensor. To verify the proposed scheme, an experimental demonstration to recognize the face's position closer than the minimum detection range of the TOF sensor is also provided.

2.2. Principles of Controlling the Ray Directions to the Face's Position

In addition to recognition of the face's position described above, accurate control of the directions of rays converging to the recognized facial position is also essential. For that purpose, we use a directional backlight system composed of a line light source and a convex-lens array with a focal length of f_{LA}, as shown in Fig. 3.

Since light rays emitted from the line light source proceed in parallel after passing through the convex-lens array, we can control the ray directions by positioning the line light source [7]. However, in an actual directional backlight system the line light source has a physical width

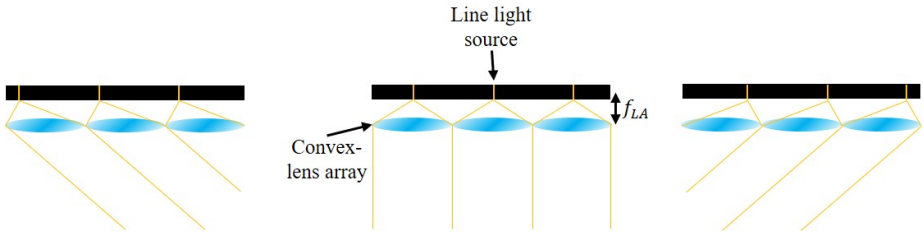

FIG. 3. Structure and principle of the directional backlight system.

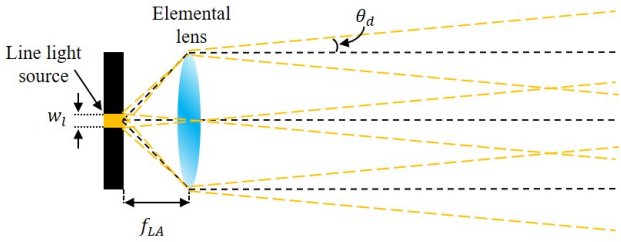

FIG. 4. Effect of the width of the line light source on the imperfect collimation.

w_l, as denoted in Fig. 4. Thus the light rays from the convex-lens array spread with a deviation angle θ_d, as derived below.

$$\theta_d = \arctan\left(\frac{w_l}{2f_{LA}}\right). \tag{5}$$

Nevertheless, since we expect that θ_d is only about 0.2 degrees in our experimental demonstration, we expect that the effect of imperfect collimation shown in Fig. 4 is negligible. Thus, using that principle, we can make all light be converged at the eye positions of a registered observer with pupil size of 2-8 mm, as shown in Fig. 5 [8].

For this purpose, we calculate the position of each line light source using a coordinate system shown in Fig. 6. When a converged position decentered by x_o from the center of the 0_{th} elemental lens, and x_n away from the n_{th} elemental lens, centers on depth z, the n_{th} line light source must be decentered by L_{pn} from the center position of the n_{th} elemental lens. Then we can derive L_{pn} as follows, using a proportional relation.

$$L_{pn} = -\frac{f_{LA}}{z}x_n. \tag{6}$$

Since L_{pn} denotes the decentered position within the n_{th} elemental lens, it is necessary to convert it with a global coordinate $L_{pn}^{'}$ using the pitch p_{el} of a single elemental lens, as follows:

$$L_{pn}^{'} = np_{el} + L_{pn}. \tag{7}$$

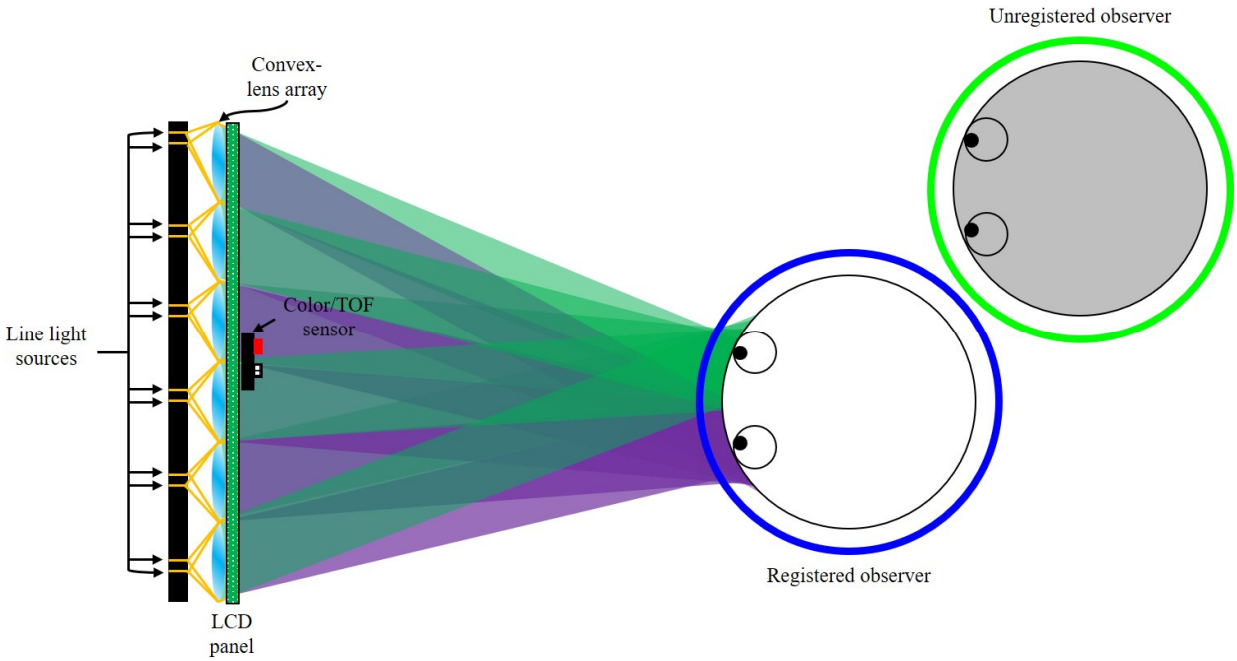

FIG. 5. Principles of the proposed privacy-protection system.

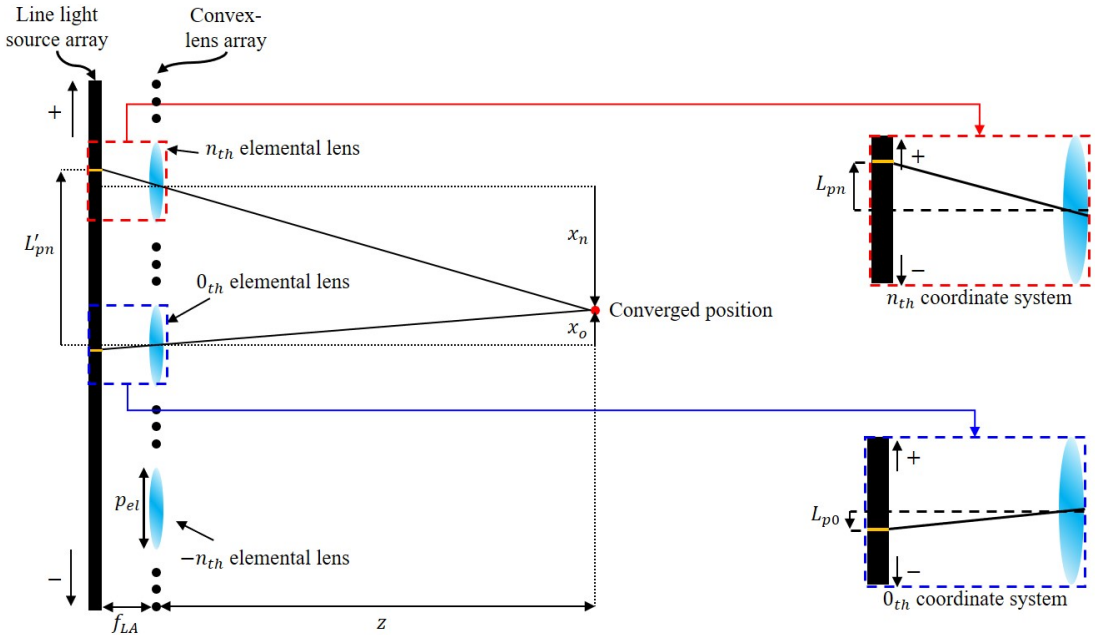

FIG. 6. Calculation of line light source positions.

Then we can use the following relation between x_n and x_o.

$$x_n = -np_{el} + x_o. \tag{8}$$

Combining the above equations, we can calculate the position of each line light source from the true position of the face's center.

$$L_{pn}^{'} = \left(\frac{f_{LA}}{z} + 1\right) np_{el} - \frac{f_{LA}}{z} x_o. \tag{9}$$

III. ANALYSIS OF THE VIEWING PARAMETERS

Since control of the ray direction is essential for the proposed system, the viewing angle is one of the most important viewing parameters. Regarding the above principles, the viewing angle $\theta_{\max}$ of the proposed system can be derived from the focal length f_{LA} of the lens array, the pitch p_{el} of a single elemental lens, the size w_{LA} of the convex-lens array, and the depth z of the recognized face from the convex-lens array shown in Fig. 7.

To derive the viewing angle, we should consider the leftmost and rightmost positions where the light rays will converge. For that purpose, the first step is to calculate the distance d_{cross} between the convex-lens array and crossing point where the leftmost/rightmost light rays meet.

$$d_{cross} = f_{LA}\left(\frac{w_{LA}}{p_{el}} - 1\right). \tag{10}$$

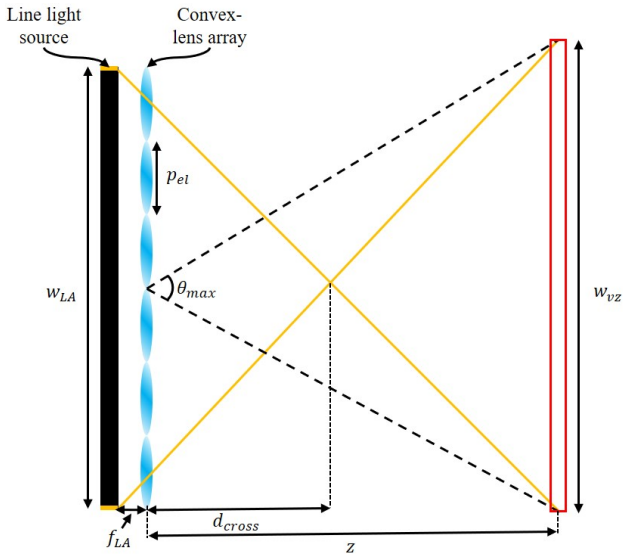

FIG. 7. Analysis of the viewing zone and viewing angle of the proposed method.

Then we can expect the maximum size w_{vz} of the viewing zone at a depth of z according to the following equation from the proportionality relation.

$$w_{vz} = (w_{LA} - p_{el})\left(\frac{z}{d_{cross}} - 1\right). \tag{11}$$

Using the above derivations, we can calculate the viewing angle $\theta_{\max}$ as follows:

$$\theta_{\max} = 2\arctan\left(\frac{w_{vz}}{2z}\right) = 2\arctan\left(\frac{1}{2}\left(p_{el}\left(\frac{1}{f_{LA}} + \frac{1}{z}\right) - \frac{w_{LA}}{z}\right)\right). \tag{12}$$

IV. EXPERIMENTAL RESULTS

Pictures of the experimental setup and face cameras are shown in Fig. 8. We use two different faces, one registered and one unregistered, and located cameras with resolution of 4032 by 3024 pixels at the position of the right eye of each face. Thus we can check whether the proposed system can ban the sight of the unregistered observer while providing proper images to the registered user only. Figure 9 shows the positions of face cameras on the registered face. Regarding that the minimum detection range of the TOF sensor is 0.7 m, we chose two positions (labeled 1 and 2) closer than that, to verify that our method works properly under any circumstance. Behind an LCD panel with a resolution of 1920 by 1080 and a pixel pitch of 0.25 mm, we attach a convex-lens array composed of 13 by 13 elemental lenses, each with pitch p_{el} of 10 mm and focal length f_{LA} of 22 mm, as shown in Fig. 9. The line light source behind the lens array has a width of 0.162 mm. From those parameters, we expect that the proposed system can provide privacy protection within a viewing angle $\theta_{\max}$ of about 17° when the observer is located 800 mm from the device. Thus, we set the leftmost and rightmost positions of the face camera located 800 mm (positions 3 and 5) from the LCD panel to be the border of the viewing zone, to verify the analysis in chapter III.

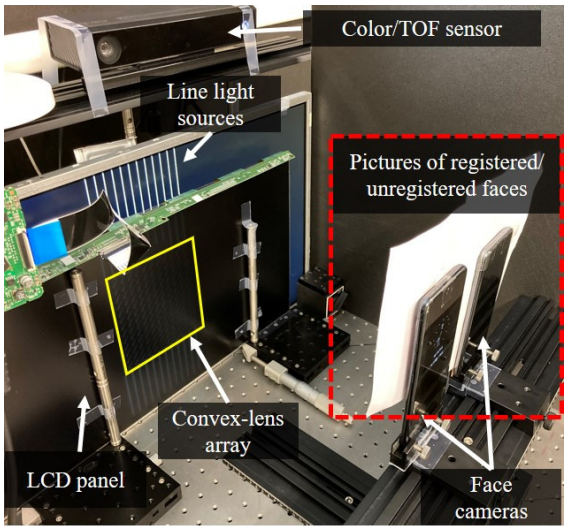

FIG. 8. Pictures of the experimental setup and face cameras, with registered and unregistered faces.

As a first step of verification, we locate two face cameras with registered and unregistered faces 800 mm from the LCD panel, and check whether the system provides the screen information only to the location of the registered face. The experimental results are shown in Fig. 10: The image displayed on the LCD panel (skull and crossbones) can be captured only at the position of the registered face (denoted with blue solid lines), whereas the face camera at the other position, which represents a visual hacker (denoted with green dashed lines), captures no information from the screen. Therefore, from the experimental results in Fig. 10, it can be verified that the proposed

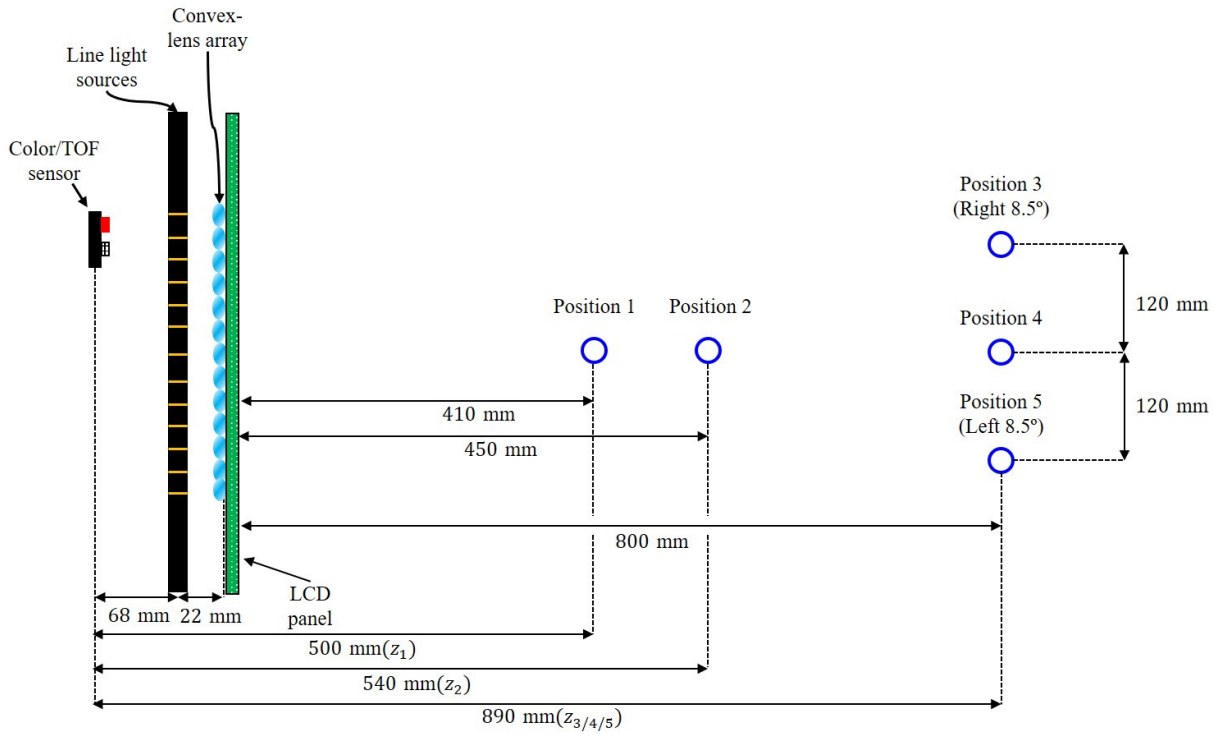

FIG. 9. Positions of the face cameras to capture the observed views.

scheme works as expected, when the observer is within the detection range of the TOF sensor.

The next verification is for a case when the observer is outside of the detection range of TOF sensor. For that purpose, we locate the face camera of the registered observer at positions 1 and 2. In this case, it is expected that the depth of the registered face is retrieved using the parameters N_{eye}, N_{eye_i}, and z_i, as denoted in Eq. (4). In the experiment, the measured depth z_i from the TOF sensor is 894 mm and N_{eye_i} is 67 pixels, when the registered face is at position 4. Then, from the measured values of N_{eye} at position 1 (121 pixels) and position 2 (111 pixels), we could retrieve the depths z_1 and z_2 as 495 mm and 540 mm from the TOF sensor respectively. Thus we can confirm that those values are well matched by the experimental conditions shown in Fig. 9. The experimental results for the second case are shown in Fig. 11: The experimental demonstration can provide the screen image only to the eye location of the registered face's camera (denoted with blue solid lines), while the unregistered face at the other position (denoted with green dashed lines) can capture no image information. Therefore, it can be concluded that the proposed scheme protects the privacy of the registered user securely, regardless of the distance between the observer and the device.

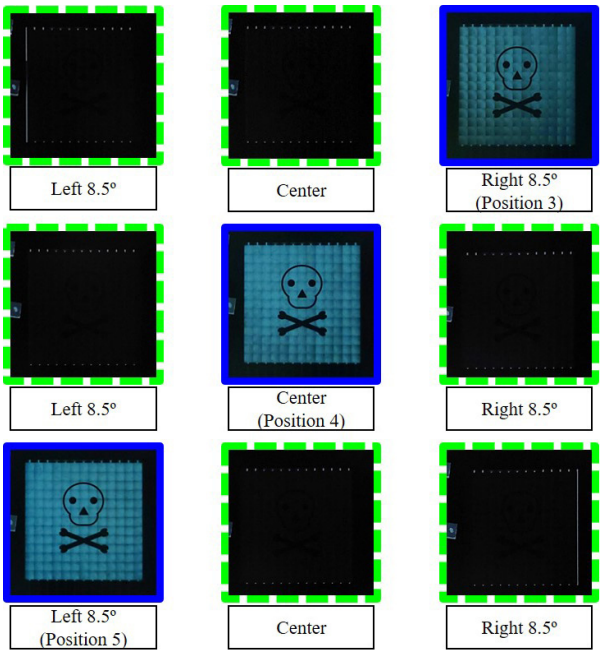

FIG. 10. Experimental results when the face camera is within the detection range of the TOF sensor. The blue solid and green dashed lines represent the locations of the registered and unregistered observers respectively.

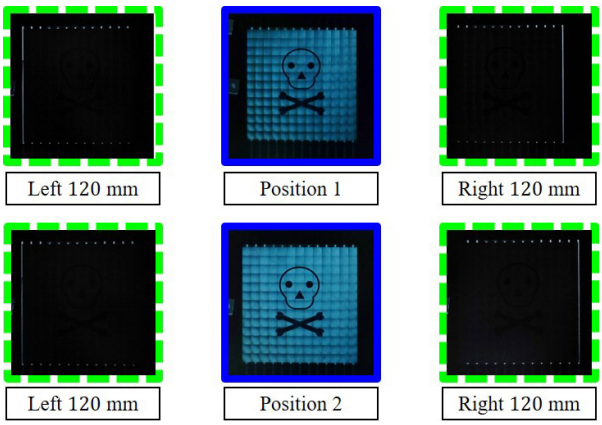

FIG. 11. Experimental results when the face camera is closer than the detection range of the TOF sensor. The blue solid and green dashed lines represent the locations of the registered and unregistered observers respectively.

V. CONCLUSION

With the rapid progress of mobile devices, the protection of the information in them becomes more important. Though various kinds of securing technology are developed in transmitting the information, the display screen is still vulnerable to simple peeping: visual hacking. In this paper, we have proposed an effective privacy-protection method to overcome the limitation of the detection range of a TOF sensor, and verified it with experimental demonstrations. We expect that the proposed system can be applied to various kinds of display devices to eliminate concerns over visual hacking.

ACKNOWLEDGMENT

This work was supported in part by the Information Technology Research Center (ITRC) support program supervised by the Institute for Information and Communications Technology Promotion (IITP) under Grant IITP-2017-2015-0-00448, and in part by the Basic Science Research Program through the National Research Foundation of Korea (NRF) funded by the Ministry of Education under Grant 2018R1D1A1B07049563.

REFERENCES

1. P. Barker, "Visual hacking - why it matters and how to prevent it," Netw. Secur. **42**, 14-17 (2019).
2. H. Yoon, S.-G. Oh, D. S. Kang, J. M. Parck, S. J. Choi, K. Y.Suh, K. Char, and H. H. Lee, "Arrays of *Lucius* microprisms for directional allocation of light and auto-stereoscopic three-dimensional displays," Nat. Commun. **2**, 455 (2011).
3. G. E. Gaides, I. A. Kadoma, D. B. Olson, R. A. Larson, and A. R. Sykora, "Light collimating film," U.S. Patent 8012567B2 (2011).

4. J.-H. Kim, C. H. Lee, S. S. Lee, and K.-C. Lee, "Highly transparent privacy filter film with image distortion," Opt. Express **22**, 29799-29804 (2014).
5. T. Guzvinecz, V. Szucs, and C. Sik-Lanyi, "Suitability of the Kinect Sensor and Leap Motion Controller—A Literature Review," Sensors **19**, 1072 (2019).
6. C. Kim, S. Yun, S-.W. Jung, and C. S. Won, "Color and depth image correspondence for Kinect v2," in *Advanced Multimedia and Ubiquitous Engineering* (Lecture Notes in Electrical Engineering Series, Vol. 352), J. H. Park, H.-C. Chao, H. Arabnia, and N. Y. Yen, eds. (Springer, Berlin, Heidelberg, Germany, 2015), pp. 111-116.
7. H. Kwon and H.-J. Choi, "A time-sequential multi-view autostereoscopic display without resolution loss using a multidirectional backlight unit and an LCD panel," Proc. SPIE **8288**, 82881Y (2012).
8. S. G. de Groot and J. W. Gebhard, "Pupil size as determined by adapting luminance," J. Opt. Soc. Am. **42**, 492-495 (1952).